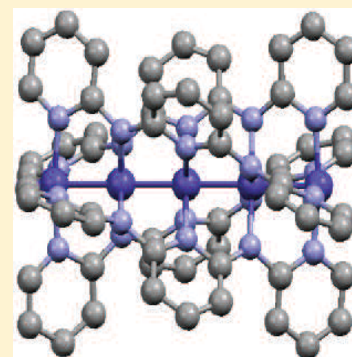


Molecular Split-Ring Resonators Based on Metal String Complexes

Yao Shen, Hsin-Yu Ko, Qing Ai, Shie-Ming Peng, and Bih-Yaw Jin*

Department of Chemistry and Center for Emerging Material and Advanced Devices and Center for Quantum Science and Engineering, National Taiwan University, Taipei 10617, Taiwan

ABSTRACT: Metal string complexes or extended metal atom chains (EMACs) belong to a family of molecules that consist of a linear chain of directly bonded metal atoms embraced helically by four multidentate organic ligands. These four organic ligands are usually made up of repeating pyridyl units, single-nitrogen-substituted heterocyclic annulenes, bridged by independent amido groups. Here, in this paper, we show that these heterocyclic annulenes are actually nanoscale molecular split-ring resonators (SRRs) that can exhibit simultaneous negative electric permittivity and magnetic permeability in the UV–vis region. Moreover, a monolayer of self-assembled EMACs is a periodic array of molecular SRRs which can be considered as a negative refractive index material. In the molecular scale, where the quantum-size effect is significant, we apply the tight-binding method to obtain the frequency-dependent permittivity and permeability of these molecular SRRs with their tensorial properties carefully considered.



INTRODUCTION

Negative refraction is an exotic refractive process which can be applied on high resolution lenses to overcome optical diffraction limits,¹ local field enhancements,² and high-sensitivity detections.^{3–5} In 1968, Veselago first investigated the electromagnetic properties of negative index material (NIM).⁶ It was not until the late 1990s that Pendry et al.^{2,7,8} introduced the use of metamaterial which allowed NIM to become a prosperous field of study. Pendry et al. also pointed out that metamaterial can be realized by a kind of conductive ring with a split pointing to a specific direction which is called split-ring resonators (SRRs).² After two years, it was experimentally realized by Shelby et al.⁹ This remarkable discovery makes SRR and metamaterial¹⁰ a new branch of research, including liquid crystal magnetic control,¹¹ cloaking,^{12,13} toroidal dipole moments,¹⁴ etc. However, metamaterials normally act on specific wavelength ranges that depend on the sizes of building circuits. For example, the experimental measurement of SRR is made in 5 mm cell dimension and operates on microwave with wavelength 3 cm.⁹ To find visible-frequency NIM, the challenge is to make arrays of SRR in nanometer scale. During the past decade, researchers have manufactured SRRs with sizes ranging from a few micrometers¹⁵ to several hundreds of nanometers.^{16–21} In this paper, we research a class of one-dimensional metal string complexes, which is also called extended metal atom chains (EMACs), for potential application as molecular-scale SRRs (MSRRs). EMACs are linear strings of transition metal atoms with four polypyridylamido ligands wrapping around them. Although there exist a number of metallic nanowires^{22,23} already, EMACs are in fact the thinnest molecular electrical wires^{24–26} that can show intriguing magnetism and large single-molecule conductances.^{27–31} Since the extended ligands of EMACs are generally pyridyl chains, they offer great configurations of well ordered arrays of conjugated rings, which can also be modeled

as Gentile oscillators of intermediate statistics.^{32–34} We wish to point out in this paper that the extended ligands of EMACs are in fact a new type of molecular SRRs. The special configuration of polypyridylamido ligands around the central metal string in EMACs makes the negative refraction possible. Moreover, due to the quantum confinement of π -electrons in the pyridyl groups, EMACs as the negative refractive index materials are promising to realize simultaneous negativity for both electric permittivity and magnetic permeability in the UV–vis region.

This paper is organized as follows: In section II, we give the theoretical derivation of the permittivity and permeability of EMACs using a simple tight-binding model. Three dimensional helical configurations of ligands are both discussed in section III. Finally, in section IV, the main results are concluded and future work is discussed.

THEORETICAL DERIVATION

Geometry of EMACs. The configuration of a one-dimensional metal string complex that consists of five transition metal atoms arranged in the linear string with twelve pyridyl units acting as molecular SRRs helically wrapping around them is shown in Figure 1. In our current study, we will treat these pyridyl units as independent quantum subsystems. For simplicity, we focus on the shortest EMACs containing only three transition metal atoms and eight molecular SRRs (see Figure 2).

Figure 2a shows the structure of a dipyridylamido ligand in a trinuclear EMAC complex. The green box presents a single heteronuclear pyridyl unit consisting of five carbon atoms (white balls) and one nitrogen atom (blue ball). We will demonstrate later that each pyridyl unit in an EMAC complex

Received: October 28, 2013

Revised: January 19, 2014

Published: January 28, 2014

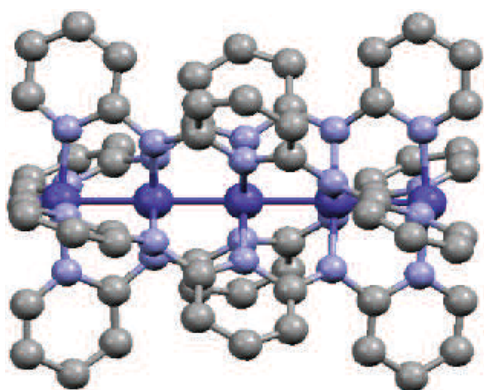


Figure 1. Linear pentanuclear chain embraced by four polypyridylamide ligands, $M_5(tpda)_4X_2$ ($tpda$ = tripyridylamide). Axial ligands are not shown. This one-dimensional metal string complex consists of five transition metal atoms (blue) and twelve single-nitrogen-substituted heterocyclic annulenes as their ligands (gray).

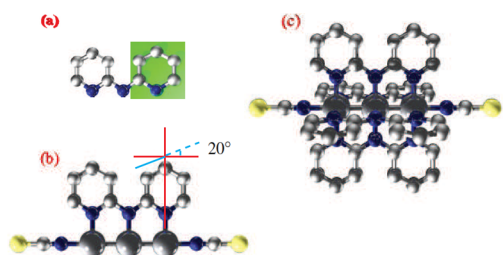


Figure 2. Pyridyl units inside a trinuclear EMAC complex. The white balls are carbon atoms. The blue balls are nitrogen atoms. The big gray balls are transition metal atoms. The two yellow balls on both ends are sulfur atoms. (a) The green box is the pyridyl unit. (b) Two split rings attach to three transition metal atoms. (c) The smallest unit of EMACs.

actually corresponds a molecular SRR. In Figure 2b, three transition metal atoms (gray balls) serve as the backbone which holds two molecular SRRs in a helical arrangement with a dihedral angle $\sim 20^\circ$ between two pyridyl units that are linked by a single amido group. With all four dipyridylamido ligands attached on the metal string with a 4-fold rotational symmetry, we get an EMAC complex (Figure 2c).

Hückel Model. The electromagnetic properties mainly originate from the response of π electrons of the ligands to the external electromagnetic fields. We label six p_z orbitals in one of the eight pyridyl groups according to Figure 3. Since each ligand consists of two pyridyl units linked by an amido group, without loss of generality, we will assume that these pyridyl units are independent and can be modeled by the Hückel model as^{36,37}

$$\mathcal{H} = \sum_{j=1}^6 \alpha_j |j\rangle \langle j| + \sum_{j=1}^6 \beta_{j,j+1} (|j\rangle \langle j+1| + |j+1\rangle \langle j|) \quad (1)$$

where $|j\rangle$ is the p_z -atomic orbital at site j with site energy α_j , $\beta_{j,j+1}$ is the coupling strength between j th and $(j+1)$ th sites. Here, the cyclic condition is employed, i.e., $|7\rangle = |1\rangle$. We assume that the only nitrogen atom is located at site 1. Therefore

$$\alpha_j = \begin{cases} \alpha_C, & \text{for } j \neq 1 \\ \alpha_N, & \text{for } j = 1 \end{cases} \quad (2)$$

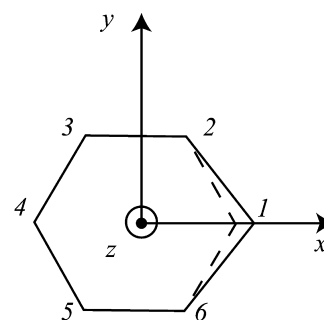


Figure 3. Schematic diagram of a pyridine molecule modeled as a perfect hexagon. The origin is set at the center of the hexagon with the z axis perpendicular to the plane. The six sites are labeled sequentially from 1 to 6, with site 1 to be a nitrogen atom and others to be carbon atoms.

$$\beta_{j,j+1} = \begin{cases} \beta_{CC}, & \text{for } j \neq 1, 6 \\ \beta_{CN}, & \text{for } j = 1, 6 \end{cases} \quad (3)$$

The Hückel Hamiltonian 1 can be diagonalized numerically as

$$\mathcal{H} = \sum_{k=1}^6 \varepsilon_k |\psi_k\rangle \langle \psi_k| \quad (4)$$

$$|\psi_k\rangle = \sum_{j=1}^6 c_{kj} |j\rangle \quad (5)$$

Each pyridyl unit contains six noninteracting π electrons. On account of the spin degrees of freedom, the ground state is the state with all six electrons filling the three lowest molecular orbitals (see Figure 4), i.e., $|\Psi_0\rangle = a_{1\uparrow}^\dagger a_{1\downarrow}^\dagger a_{2\uparrow}^\dagger a_{2\downarrow}^\dagger a_{3\uparrow}^\dagger a_{3\downarrow}^\dagger |\text{vac}\rangle$, with

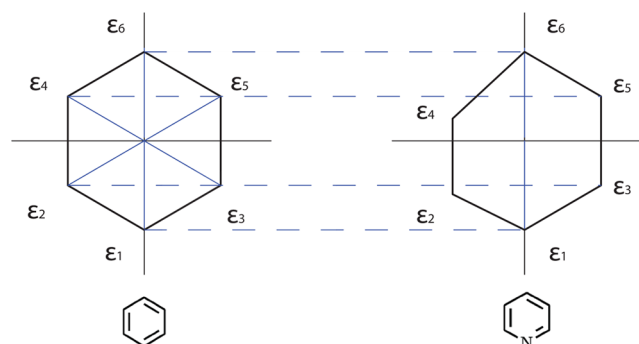


Figure 4. Spectra of (left) benzene and (right) pyridine molecules. Due to the symmetry, there are two sets of 2-fold degenerate states for a benzene molecule, i.e., $|\psi_2\rangle$ and $|\psi_3\rangle$, and $|\psi_4\rangle$ and $|\psi_5\rangle$. Because a carbon atom is substituted by a nitrogen atom, the symmetry is broken and thus there are no degenerate states for a pyridine molecule.

the total π electron energy $E_0 = 2(\varepsilon_1 + \varepsilon_2 + \varepsilon_3)$. Here $a_{k\uparrow(\downarrow)}^\dagger$ creates an electron in the molecular orbital $|\psi_k\rangle$ with spin up(down) and $|\text{vac}\rangle$ corresponds to the vacuum state.

Within the independent electron approximation, the ground state is coupled, through the external electromagnetic field, to single excitation states by promoting one electron from occupied to unoccupied molecular orbitals. There are eighteen single excitation states $|\Psi_I\rangle = |\Psi_{a\sigma}^{\sigma\sigma}\rangle = a_{r\sigma}^\dagger a_{a\sigma} |\Psi_0\rangle$, $a = 1, 2, 3$, $r = 4, 5, 6$ and $\sigma = \uparrow, \downarrow$, with eigen-energies $E_I = \langle \Psi_{a\sigma}^{\sigma\sigma} | \mathcal{H} | \Psi_{a\sigma}^{\sigma\sigma} \rangle = E_0 + \varepsilon_r - \varepsilon_a$. Therefore, for six noninteracting π electrons in the absence of applied electromagnetic field, the Hamiltonian reads

$$H_0 = \sum_{I=0}^{18} E_I |\Psi_I\rangle \langle \Psi_I| \quad (6)$$

Perturbation Theory in Rotating Frame. In the presence of a time-dependent electromagnetic field, the total Hamiltonian including the interaction between the electrons and the field is

$$\begin{aligned} H &= H_0 - \vec{\mu} \cdot \vec{E}(\vec{r}, t) - \vec{m} \cdot \vec{B}(\vec{r}, t) \\ &= H_0 - \vec{\mu} \cdot \vec{E}_0 \cos(\vec{k} \cdot \vec{r} - \omega t) - \vec{m} \cdot \vec{B}_0 \cos(\vec{k} \cdot \vec{r} - \omega t) \\ &\simeq H_0 - \vec{\mu} \cdot \vec{E}_0 \cos(\omega t) - \vec{m} \cdot \vec{B}_0 \cos(\omega t) \end{aligned} \quad (7)$$

where $\vec{\mu}$ and \vec{m} are the electric and magnetic dipole moments, respectively. In the last line we have assumed the wavelength of the field is much larger than the size of the molecule, i.e., $\vec{k} \cdot \vec{r} \simeq 0$ if the origin of the coordinate is chosen at the center of the molecule.

Then, after transforming to the rotating frame defined by a unitary transformation, $U^\dagger = \exp(-i\omega t |\Psi_0\rangle \langle \Psi_0|)$, and we have used the rotating wave approximation, the effective Hamiltonian becomes

$$\begin{aligned} H' &= U^\dagger H U + iU^\dagger \dot{U} \\ &\simeq \sum_{I=1}^{18} E_I |\Psi_I\rangle \langle \Psi_I| + (E_0 + \omega) |\Psi_0\rangle \langle \Psi_0| + H'_1 \end{aligned} \quad (8)$$

where

$$\begin{aligned} H'_1 &= -\frac{1}{2} \sum_{I=1}^{18} (\vec{\mu}_{I0} \cdot \vec{E}_0 |\Psi_I\rangle \langle \Psi_0| + \vec{\mu}_{0I} \cdot \vec{E}_0 |\Psi_0\rangle \langle \Psi_I|) \\ &\quad - \frac{1}{2} \sum_{I=1}^{18} (\vec{m}_{I0} \cdot \vec{B}_0 |\Psi_I\rangle \langle \Psi_0| + \vec{m}_{0I} \cdot \vec{B}_0 |\Psi_0\rangle \langle \Psi_I|) \end{aligned} \quad (9)$$

where $\vec{\mu}_{II'} = \langle \Psi_I | \vec{\mu} | \Psi_{I'} \rangle$ and $\vec{m}_{II'} = \langle \Psi_I | \vec{m} | \Psi_{I'} \rangle$. Notice that due to the transformation, the wave function $|\Psi\rangle$ and operator A in the Schrödinger picture are transformed according to $|\Psi'\rangle = U^\dagger |\Psi\rangle$ and $A' = U^\dagger A U$. Thus, the dipole operator in the rotating frame reads

$$\vec{\mu}' = \sum_{I=1}^{18} (\vec{\mu}_{I0} e^{i\omega t} |\Psi_I\rangle \langle \Psi_0| + \vec{\mu}_{0I} e^{-i\omega t} |\Psi_0\rangle \langle \Psi_I|)$$

The ground state of the effective Hamiltonian, H' , is

$$|\Psi'_0\rangle = |\Psi_0\rangle + \sum_{I=1}^{18} \frac{\langle \Psi_I | H'_1 | \Psi_0 \rangle}{E_0 + \omega - E_I} |\Psi_I\rangle \quad (10)$$

The expectation value of the dipole operator for the ground state is

$$\langle \Psi'_0 | \vec{\mu}' | \Psi'_0 \rangle = -Re \sum_{I=1}^{18} \frac{\vec{\mu}_{I0} \cdot \vec{E}_0}{E_0 + \omega - E_I} \vec{\mu}_{0I} e^{-i\omega t} \quad (11)$$

If there are N identical molecules but each one with a different orientation in the total volume V , the total electric displacement field is

$$\begin{aligned} \vec{D} &= \vec{\epsilon}_0 \vec{E}_0 + \frac{\vec{P}}{V} \\ &= \vec{\epsilon}_0 \vec{E}_0 - \frac{1}{V} \sum_{n=1}^N \sum_{I=1}^{18} \frac{[\vec{\mu}_{I0}(n) \cdot \vec{E}_0] \vec{\mu}_{0I}(n)}{(E_0 + \omega - E_I)} \\ &\equiv \vec{\epsilon} \vec{E}_0 \end{aligned} \quad (12)$$

where

$$\begin{aligned} \epsilon_{ij} &\equiv \epsilon_0 \delta_{ij} - \frac{1}{V} \sum_{n=1}^N \sum_{I=1}^{18} \frac{\mu_{0I}^{(i)}(n) \mu_{I0}^{(j)}(n)}{(E_0 + \omega - E_I)}, \quad \text{for} \\ & i, j = x, y, z \end{aligned} \quad (13)$$

$$\vec{\mu}_{II'}(n) = \mu_{II'}^{(x)}(n) \hat{e}_x + \mu_{II'}^{(y)}(n) \hat{e}_y + \mu_{II'}^{(z)}(n) \hat{e}_z \quad (14)$$

and $\vec{\mu}(n)$ is the n th molecular electric dipole operator, \hat{e}_i is the unit vector of the lab coordinate system.

In order to obtain the relative dielectric constant of the material, we have to transform back to the lab coordinate system. The relation between the electric field in the molecular coordinate system \vec{E}^M and the lab coordinate system \vec{E}^L is (see Figure 5)

$$\vec{E}^L = R^{-1}(\alpha_n, \beta_n, \gamma_n) \vec{E}^M \quad (15)$$

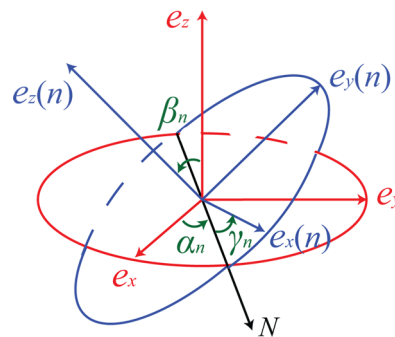


Figure 5. Matrix $R(\alpha_n, \beta_n, \gamma_n)$ corresponding to the rotation from the lab coordinate system $(\hat{e}_x, \hat{e}_y, \hat{e}_z)$ to the n th molecule coordinate system $(\hat{e}_x(n), \hat{e}_y(n), \hat{e}_z(n))$. \hat{N} is the line of nodes. α_n , β_n , and γ_n are respectively the angle between \hat{e}_x and \hat{N} , the angle between \hat{e}_z and $\hat{e}_z(n)$, and the angle between \hat{N} and $\hat{e}_x(n)$.

where

$$R(\alpha_n, \beta_n, \gamma_n) = R_z(\gamma_n) R_x(\beta_n) R_z(\alpha_n) \quad (16)$$

$$R_x(\beta_n) = \begin{pmatrix} 1 & 0 & 0 \\ 0 & \cos \beta_n & -\sin \beta_n \\ 0 & \sin \beta_n & \cos \beta_n \end{pmatrix} \quad (17)$$

$$R_z(\alpha_n) = \begin{pmatrix} \cos \alpha_n & -\sin \alpha_n & 0 \\ \sin \alpha_n & \cos \alpha_n & 0 \\ 0 & 0 & 1 \end{pmatrix} \quad (18)$$

are the rotations around $x(z)$ axis with an angle $\beta_n(\alpha_n)$, α_n , β_n , γ_n are respectively the angle between \hat{e}_x and \hat{N} , the angle between \hat{e}_z and $\hat{e}_z(n)$, and the angle between \hat{N} and $\hat{e}_x(n)$, where \hat{N} is the line of nodes. Finally, the relative dielectric constant of the material in the lab coordinate system is

$$\begin{aligned} \varepsilon_{ij}^r &\equiv \delta_{ij} - \sum_{n=1}^N \sum_{k=1}^{18} \left\{ [R^{-1}(\alpha_n, \beta_n, \gamma_n) \vec{\mu}_{0I}(n)] \cdot \hat{e}_i [R^{-1}(\alpha_n, \beta_n, \gamma_n) \vec{\mu}_{10}(n)] \cdot \hat{e}_j \right\} / \{ \varepsilon_0 V(E_0 + \omega - E_I) \}, \\ &\text{for } i, j = x, y, z \end{aligned} \quad (19)$$

From now on, we consider the magnetic response of the EMACs to the external electromagnetic field.⁴⁰ The magnetic dipole operator is related to the orbital angular momentum operator \vec{L} of π electrons through the relation, $\vec{m} = -e\vec{L}/2m_e$, where $-e$ and m_e are respectively the electric charge and mass of the π electron. Working in the molecular coordinate system, one can show that the only nonvanishing component of the angular momentum operator is along the perpendicular direction to the pyridyl plane, i.e.

$$L_x = L_y = 0 \quad (20)$$

$$\begin{aligned} L_z &= r^x p^y - r^y p^x \\ &= \frac{1}{2}(r^x p^y + p^y r^x - r^y p^x - p^x r^y) \\ &= im_e(r^x H_0 r^y - r^y H_0 r^x) \end{aligned} \quad (21)$$

where we used the relation $p^\alpha = m_e \dot{r}^\alpha = im_e [H_0, r^\alpha]$, $\alpha = x, y$.³⁸ Therefore, the magnetic dipole operator in the molecular coordinate system is given by

$$\begin{aligned} \vec{m} &= \frac{-e}{2m_e} L_z \hat{e}_z \\ &= \frac{-ie}{2} \hat{e}_z (r^x H_0 r^y - r^y H_0 r^x) \\ &= \frac{-ie}{2} \hat{e}_z \sum_{k,k'} \sum_{k_1} E_{k_1} (r_{kk_1}^x r_{k_1 k'}^y - r_{kk_1}^y r_{k_1 k'}^x) |\Psi_k\rangle \langle \Psi_{k'}| \end{aligned} \quad (22)$$

where

$$r_{II'}^\alpha = \langle \Psi_I | r^\alpha | \Psi_{I'} \rangle \quad (23)$$

Notice that as r^α is a single-electron operator and two different excited states $|\Psi_I\rangle$ and $|\Psi_{I'}\rangle$ differ from each other by two single-electron states, $|\Psi_I\rangle$ and $|\Psi_{I'}\rangle$ should not be two different excited states.³⁹

Similarly, since

$$\langle \Psi_0 | \vec{m} | \Psi_0 \rangle = -Re \sum_{I=1}^{18} \frac{\vec{m}_{10} \cdot \vec{B}_0}{E_0 + \omega - E_I} \vec{m}_{0I} e^{-i\omega t} \quad (24)$$

the magnetic response is

$$\begin{aligned} \vec{B} &= \vec{\mu}_0 \vec{H}_0 + \vec{\mu}_0 \frac{\vec{M}}{V} \\ &= \vec{\mu}_0 \vec{H}_0 - \sum_{n=1}^N \sum_{I=1}^{18} \frac{\mu_0 \vec{m}_{10}(n) \cdot \vec{B}_0}{V(E_0 + \omega - E_I)} \vec{m}_{0I}(n) \\ &\equiv \vec{\mu} \vec{H}_0 \end{aligned} \quad (25)$$

and the relative permeability of the material in the lab coordinate system is

$$\begin{aligned} \mu_{ij}^r &\equiv \delta_{ij} - \mu_0 \sum_{n=1}^N \sum_{k=1}^{18} \left\{ [R^{-1}(\alpha_n, \beta_n, \gamma_n) \vec{m}_{0k}(n)] \cdot \hat{e}_i [R^{-1}(\alpha_n, \beta_n, \gamma_n) \vec{m}_{k0}(n)] \cdot \hat{e}_j \right\} / \left\{ V(E_0 + \omega - E_k) \right\} \end{aligned} \quad (26)$$

for $i, j = x, y, z$.

Permittivity and Permeability. As the symmetric center is chosen as the origin of coordinate, the nuclear contribution can be neglected and thus the electric dipole moment operator is

$$\vec{\mu} = - \sum_{j=1}^6 e \vec{r}_j \quad (27)$$

where \vec{r}_j is the position vector of j th π electron. According to ref. 39, for the case with single-electron operators, the matrix elements are given by

$$\langle \Psi_0 | \vec{\mu} | \Psi_I \rangle = \langle \Psi_0 | \vec{\mu} | \Psi_{a\sigma}^{r\sigma} \rangle = -e \langle \Psi_a | \vec{r} | \Psi_r \rangle = -e \vec{r}_{ar} \quad (28)$$

Here

$$\langle \Psi_a | \vec{r} | \Psi_r \rangle = \sum_{j=1}^6 c_{aj}^* c_{rj} \vec{R}_j \quad (29)$$

where \vec{R}_j is the position of j th site in the lab coordinate system. The magnetic dipole moment operator is

$$\vec{m} = -\frac{ie}{2} \hat{e}_z \sum_{I \neq 0} (E_I - E_0) (r_{II'}^x r_{I0}^y - r_{II'}^y r_{I0}^x) |\Psi_I\rangle \langle \Psi_0| + \text{h.c.} \quad (30)$$

where we have used the relation $\vec{r}_{II'} = 0$ if $I \neq I'$ and both I and I' are not equal to zero.

■ RESULT AND DISCUSSION

General Result of Permittivity and Permeability.

Equations 19 and 26 derived in the previous section will be employed here to show that a material consisting of EMAC complexes can exhibit negative permittivity and permeability simultaneously in the UV-vis region. For anisotropic material in an electromagnetic field with arbitrary direction, the permittivity and permeability are generally second rank tensors. In our numerical simulation, we use the following parameters³⁵ for the π electrons, i.e., the site energies $\alpha_C = 0$, $\alpha_N = \alpha_C + 0.5\beta_{CC}$, the coupling strengths $\beta_{CC} = -3.6$ eV, $\beta_{CN} = 0.8\beta_{CC}$ and the excited-state lifetime $\tau = 0.1$ μ s. And the rotation angles for two successive pyridyl groups in the smallest trimetal EMACs are $\alpha_n = 0.105$, $\beta_n = 0.829$, $\gamma_n = -0.105$. We rotate the tensors of ε and μ to a special coordinate system, in which ε is diagonalized. In this special coordinate system, μ has very small off-diagonal terms. Therefore, we only consider the diagonal terms of μ . The results of computation of electric permittivity and magnetic permeability tensors along three principal axes are shown in Figure 5. Due to the 4-fold rotational symmetry of the EMAC complexes, one principal axis (q axis) of the dielectric permittivity ellipsoid coincides with the central metal string, while the other two axes (o and p axes) point to the perpendicular lateral directions. In addition, because of the 4-fold rotational symmetry of the EMAC complexes, the dielectric permittivity (magnetic permeability) along the two lateral axes are equal. Moreover, it is interesting to note that the component along the central metal string for the dielectric

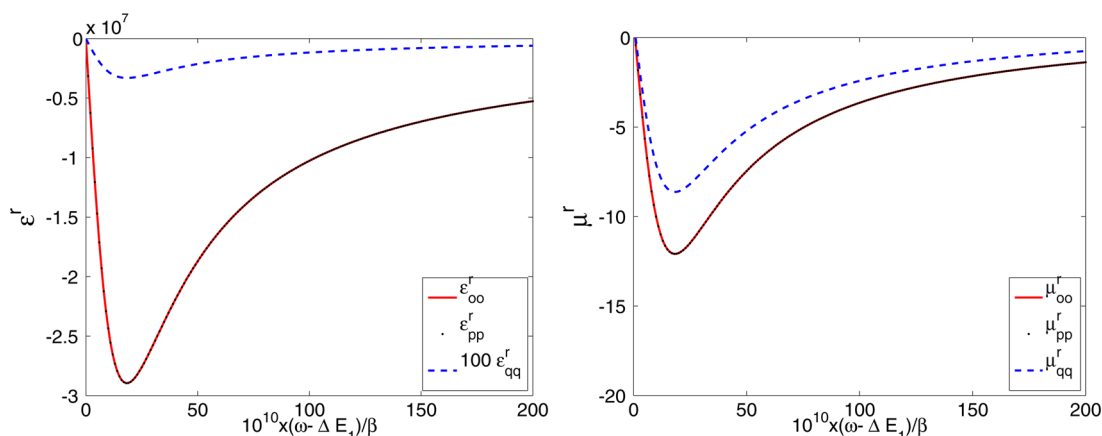


Figure 6. (left) Permittivity and (right) permeability of EMACs. The horizontal and vertical coordinates are two dimensionless quantities. They are frequency, permittivity and permeability respectively. The three color lines demonstrate three eigenvalues of permittivity and permeability tensor. The permittivity and permeability along o , p , and q directions (see Figure 7) are all negative here. Thus we have three-dimensional negative permittivity and permeability.

permittivity is significantly smaller than the other two components lying perpendicular to the central metal string, as will be explained in the next section. Apparently, the permittivity and permeability of EMACs are simultaneously negative in all these three principal directions. As a result, for any given direction, since negative refraction will occur in certain frequency window where ϵ and μ are simultaneously negative, EMACs are three-dimensional NIM material. Generally speaking, in the experimental investigations it is difficult to align the molecules in a specific direction. For an arbitrary direction, the permittivity and permeability can be approximated by the diagonal terms as long as the off-diagonal terms are sufficiently small. In this case, we could observe the negative refractive index for both negative diagonal terms of the permittivity and permeability.

In Figure 6, we only show the numerical results for the negative refraction around the first transition frequency, i.e., ω

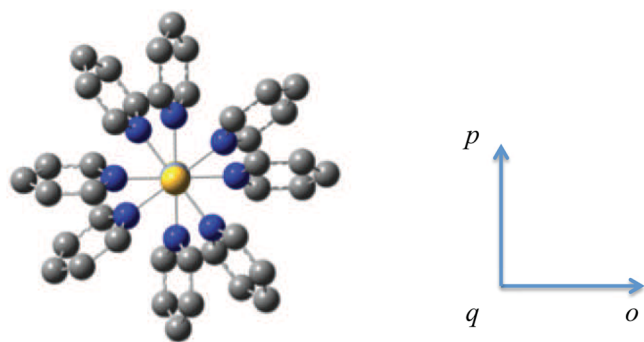


Figure 7. Main axes of the permittivity and permeability of EMACs. The o , p , and q axes in this figure are the main directions of ϵ and μ which are different from those axes in Figure 3

$\sim E_1 - E_0$, where contributions are mainly from the transition dipole moments, μ_{01} and m_{01} . In general, the negative refraction can also occur around other transition frequencies, but the widths of the negative refraction are much narrower. Besides, according to our numerical simulation, which is not shown here, the width of the negative refraction window is very sensitive to the excited state lifetime. For a sufficiently small τ ,

the window width might be greatly reduced and the negative refraction may even disappear.

We also wish to point out that, unlike the traditional microscale SRRs, quantum confinement in molecular SRRs plays an important role on the response frequency where negative refraction occurs. It is known for a long time that the fundamental wavelength of electromagnetic field absorbed by a classical metallic particle or antenna with length L is given by $\lambda = 2L$; while the wavelength absorbed by molecular-scale quasi-metallic objects or unsaturated molecules such as conjugated polyenes is $\lambda = 400L$, which is much larger than the length of polyenes due to the quantum confinement effect.^{56,57} It is interesting to note that similar trend is also observed in the response frequency where negative refraction occurs by many experimental and theoretical investigations as shown in Figure 8. Basically, the classical metamaterials based on the different

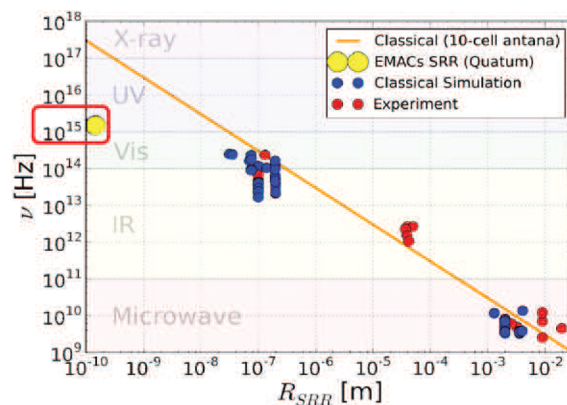


Figure 8. Quantum effect on the response frequency of negative refractive index. The data for classical materials (blue and red points) in this figure are supported by refs 2 and 41–54.

sizes of SRRs show a good linear relationship between response frequency and their dimensions on the log–log plot. When the dimension of SRRs is shrunk to the nanometer scale, by simple extrapolation of the classical linear relationship, we would expect the negative indexes to occur in the frequency domain far higher than the UV–vis frequency, which is of course incorrect. Instead, the negative indexes of EMAC complexes in

the near-ultraviolet regime can only be explained by the quantum confinement effect. In the case of EMAC complexes, a pyridine molecule is about a nanometer, whose response frequency is hundreds of times smaller than that predicted by the classical theory. This suggests that for visible/near-ultraviolet light we could obtain a meta-material of negative indexes with significantly smaller volume, i.e., $\sim 10^{-6}$, as compared to the classical meta-material. Therefore, the promising meta-material made by EMAC complexes would gain much advantage over its classical counterpart as it can be made sufficiently smaller.

PMO Analysis. In order to understand the structure–property relationship more clearly, here in this section, we perform the standard perturbation molecular orbital (PMO) theory.⁵⁵ We start from the simple Hückel description of a benzene molecule, where all site energies and resonance integrals are equal

$$\mathcal{H}_B = \alpha \sum_{j=1}^6 |j\rangle\langle j| + \beta \sum_{j=1}^6 (|j\rangle\langle j+1| + |j+1\rangle\langle j|) \quad (31)$$

Here $N = 6$ is the total number of sites in a benzene molecule. Extension to other $N(= 4n + 2)$ -annulenes can be done straightforwardly. Taking a discrete Fourier transform $|k\rangle = (1/\sqrt{6})\sum_{j=1}^6 e^{-ikj}|j\rangle$, $k = m\pi/3$ and $m = -3, -2, \dots, 2$, \mathcal{H}_B can be diagonalized as $\mathcal{H}_B = \sum_k \varepsilon_k^{(0)}|k\rangle\langle k|$, where $\varepsilon_k^{(0)} = \alpha + 2\beta\cos k$. In the case of a benzene molecule, $k_1 = -\pi$ and $k_4 = 0$ correspond to the lowest and the highest molecular orbitals, respectively, while $k_{2,6} = \mp 2\pi/3$ and $k_{3,5} = \mp \pi/3$ correspond to two sets of degenerate frontier molecular orbitals, respectively.

In the PMO analysis, a pyridine molecule is analyzed by making a chemical perturbation on its parent molecule, i.e. a benzene. Within the Hückel framework, replacing a carbon atom by a nitrogen atom at site 1 is equivalent to introducing a perturbation term, i.e. $\mathcal{H}_p = \mathcal{H}_B + \mathcal{V}$, where

$$\mathcal{V} = \Delta\alpha|1\rangle\langle 1| + \Delta\beta(|1\rangle\langle 2| + |6\rangle\langle 1|) + \text{h.c.} \quad (32)$$

Transforming to the delocalized orbital representation through the discrete Fourier transform, we get

$$\mathcal{H}_p = \sum_k (\varepsilon_k^{(0)} + \delta\varepsilon_k)|k\rangle\langle k| + \sum_{k < k'} J_{kk'}|k\rangle\langle k'| + \text{h.c.} \quad (33)$$

where the diagonal and off-diagonal perturbations terms are related to original chemical perturbations $\Delta\alpha$ and $\Delta\beta$ by

$$\delta\varepsilon_k = \frac{\Delta\alpha}{6} + \frac{2\Delta\beta}{3} \cos k \quad (34)$$

$$J_{kk'} = \frac{\Delta\alpha}{N} \cos(k - k') + \frac{2\Delta\beta}{N} [\cos(k - 2k') + \cos(kN - k')] \quad (35)$$

and they correspond to the first-order and higher-order perturbation corrections to the energies of molecular orbital energies, respectively. Note that the degeneracies are not removed by the diagonal terms, i.e., $\delta\varepsilon_2 = \delta\varepsilon_6$ and $\delta\varepsilon_3 = \delta\varepsilon_5$. Incorporating the couplings between the degenerate molecular orbitals, the unperturbed Hamiltonian can be analytically diagonalized as

$$\begin{aligned} \mathcal{H}_p &= \sum_k \varepsilon_k |k\rangle\langle k| + J_{k_2 k_6} |k_2\rangle\langle k_6| + J_{k_3 k_5} |k_3\rangle\langle k_5| + \text{h.c.} \\ &= \sum_k \varepsilon_k' |\tilde{k}\rangle\langle \tilde{k}| \end{aligned} \quad (36)$$

where $\varepsilon_k = \varepsilon_k^{(0)} + \delta\varepsilon_k$, for $k = k_1, k_4$, $\varepsilon_k' = \varepsilon_k$ and $|\tilde{k}\rangle = |k\rangle$, for other k 's, we have $\varepsilon_{k_2}'\varepsilon_{k_6}' = \varepsilon_{k_2} \mp J_{k_2 k_6}$, $\varepsilon_{k_3}'\varepsilon_{k_5}' = \varepsilon_{k_3} \mp J_{k_3 k_5}$, and $|\tilde{k}_2\rangle, |\tilde{k}_6\rangle = (\mp|k_2\rangle + |k_6\rangle)/\sqrt{2}$, $|\tilde{k}_3\rangle, |\tilde{k}_5\rangle = (\mp|k_3\rangle + |k_5\rangle)/\sqrt{2}$. The couplings between two degenerate pairs are respectively $J_{k_2 k_6} = (2\Delta\beta - \Delta\alpha)/6 = -0.1\beta_{CC}/12$ and $J_{k_3 k_5} = -(2\Delta\beta + \Delta\alpha)/12 = -0.9\beta_{CC}/12$. The matrix elements of dipole operator for the transition to the lowest excited state can also be evaluated straightforwardly

$$\langle \Psi_1 | \vec{\mu} | \Psi_0 \rangle \propto \langle \tilde{k}_3 | \vec{r} | \tilde{k}_6 \rangle = \frac{\sqrt{3}i}{2} (\vec{R}_1 + \vec{R}_2) \quad (37)$$

where we have made use of $\vec{R}_{j+3} = -\vec{R}_j$. Because $\langle \tilde{k}_3 | \vec{r} | \tilde{k}_6 \rangle$ has a greater component in the x direction than in the y direction, we would expect $\varepsilon_{oo(pp)}'$ to be sufficiently larger than ε_{qq}^r .

On the other hand, due to the symmetry of the unperturbed Hamiltonian \mathcal{H}_B , the diagonal matrix elements of the displacement operator vanish, i.e.

$$\langle k | \vec{r} | k \rangle = 0 \quad (38)$$

As a result, all $\langle \psi_k | \vec{r} | \psi_k \rangle$'s disappear to the present order, and their contribution originates from the next order due to the presence of \mathcal{V} . It also suggests that due to the presence of nitrogen atom, the one-atom-substituted Hückel model makes an SSR and thus can interact with the applied magnetic field.

Besides, we also remark that the molecular SSR can be realized by molecules other than EMACs. For example, (P)-2,2'-biphenol⁵⁸ is two connected phenol where a hydrogen atom of benzene is replaced by a hydroxyl group. In this molecule, due to the presence of a hydroxyl group, the site energy and two coupling constants of the connected carbon atom are modified. Furthermore, since the two phenol are not in the same plane, this molecule could respond to the electromagnetic field in all three dimensions. Another possible candidate is 2,5-dichloropyrazine⁵⁹ where two nitrogen atoms are substituted for two carbon atoms and two hydrogen atoms are replaced by two chlorine atoms. In this molecule, due to this chemical tuning, the energy spectrum of the excited states is significantly adjusted. Therefore, our proposal may work not only in EMACs but also in molecules with a SRR configuration.

CONCLUSION

In this paper, we discover a new family of conjugated molecules that have the potential to exhibit negative refractive index in the UV–vis region. The molecules of interest are single-nitrogen-substituted heterocyclic annulenes, in which heteroatoms serve as splits to turn on magnetic resonance as their classical analogue. With heterocyclic annulenes as molecular split-ring resonators (SSRs), we show that extended metal atom chains (EMACs) can realize negative permittivity and permeability simultaneously in quantum regime. A simple tight-binding calculation based on linear response within the electric and magnetic dipole approximations gives a reasonable estimate of the negative index region of the three-dimensional and helical arrangement of these molecular SSRs. Although we have adopted a simplified independent electron model, the

Coulombic interaction between electrons should not destroy the prediction of negative refraction. Furthermore, besides EMACs, a family of single-nitrogen-substituted heterocyclic annulenes may also serve as the negative refraction materials if the molecules are appropriately arranged.

AUTHOR INFORMATION

Corresponding Author

*E-mail: byjin@ntu.edu.tw.

Notes

The authors declare no competing financial interest.

ACKNOWLEDGMENTS

The research was supported by the National Science Council, Taiwan and the Center of Theoretical Sciences of National Taiwan University.

REFERENCES

- (1) Pendry, J. B. Negative Refraction Makes a Perfect Lens. *Phys. Rev. Lett.* **2000**, *85*, 3966–3969.
- (2) Pendry, J. B.; Holden, A. J.; Robbins, D. J.; Stewart, W. J. Magnetism from Conductors and Enhanced Nonlinear Phenomena. *IEEE Trans. Microwave Theory Technol.* **1999**, *47*, 2075–2084.
- (3) Cubukcu, E.; Zhang, S.; Park, Y.-S.; Bartal, G.; Zhang, X. Split Ring Resonator Sensors for Infrared Detection of Single Molecular Monolayers. *Appl. Phys. Lett.* **2009**, *95*, 043113–043113.
- (4) Clark, A. W.; Glidle, A.; Cumming, D. R. S.; Cooper, J. M. Plasmonic Split-Ring Resonators as Dichroic Nanophotonic DNA Biosensors. *J. Am. Chem. Soc.* **2009**, *131*, 17615–17619.
- (5) Pryce, I. M.; Kelaita, Y. A.; Aydin, K.; Briggs, R. M.; Atwater, H. A. Compliant Metamaterials for Resonantly Enhanced Infrared Absorption Spectroscopy and Refractive Index Sensing. *ACS Nano* **2011**, *5*, 8167–8174.
- (6) Veselago, V. G. The Electrodynamics of Substances with Simultaneously Negative Values of ϵ and μ . *Sov. Phys. Uspekhi* **1968**, *10*, 509–514.
- (7) Pendry, J. B.; Holden, A. J.; Stewart, W. J.; Youngs, I. Extremely Low Frequency Plasmons in Metallic Mesostructures. *Phys. Rev. Lett.* **1996**, *76*, 4773–4776.
- (8) Pendry, J. B.; Holden, A. J.; Robbins, D. J.; Stewart, W. J. Low Frequency Plasmons in Thin-Wire Structures. *J. Phys.: Condens. Matter* **1998**, *10*, 4785–4809.
- (9) Shelby, R. A.; Smith, D. R.; Schultz, S. Experimental Verification of a Negative Index of Refraction. *Science* **2001**, *292*, 77–79.
- (10) Ropp, C.; Cummins, Z.; Probst, R.; Qin, S. J.; Fourkas, J. T.; Shapiro, B.; Waks, E. Positioning and Immobilization of Individual Quantum Dots with Nanoscale Precision. *Nano Lett.* **2010**, *10*, 4673–4679.
- (11) Zhang, F.; Zhao, Q.; Kang, L.; Gaillot, D. P.; Zhao, X.; Zhou, J.; Lippens, D. Microwave Conference, 2008. EuMC 2008. 38th European 2008; Vol. 1, pp 801–804.
- (12) Pendry, J. B.; Schurig, D.; Smith, D. R. Controlling Electromagnetic Fields. *Science* **2006**, *312*, 1780–1782.
- (13) Schurig, D.; Mock, J. J.; Justice, B. J.; Cumber, S. A.; Pendry, J. B.; Starr, A. F.; Smith, D. R. Metamaterial Electromagnetic Cloak at Microwave Frequencies. *Science* **2006**, *314*, 977–980.
- (14) Kaelberer, T.; Fedotov, V. A.; Papasimakis, N.; Tsai, D. P.; Zheludev, N. I. Toroidal Dipolar Response in a Metamaterial. *Science* **2010**, *330*, 1510–1512.
- (15) Smith, D. R.; Pendry, J. B.; Wiltshire, M. C. K. Metamaterials and Negative Refractive Index. *Science* **2004**, *305*, 788–792.
- (16) Decker, M.; Linden, S.; Wegener, M. Coupling Effects in Low-Symmetry Planar Split-Ring Resonator Arrays. *Opt. Lett.* **2009**, *34*, 1579–1581.
- (17) Pryce, I. M.; Aydin, K.; Kelaita, Y. A.; Briggs, R. M.; Atwater, H. A. Highly Strained Compliant Optical Metamaterials with Large Frequency Tunability. *Nano Lett.* **2010**, *10*, 4222–4227.
- (18) Chen, W. T.; Wu, P. C.; Chen, C. J.; Hsiao, C. T.; Yang, K.-Y.; Sun, S.; Zhou, L.; Guo, G.-Y.; Zheludev, N. I.; Tsai, D. P. Optical Magnetic Response of Upright Plasmonic Molecules in 3D Metamaterial. SPIE Newsroom 2011.
- (19) Liu, N.; Liu, H.; Zhu, S.; Giessen, H. Stereometamaterials. *Nat. Photonics* **2009**, *3*, 157–162.
- (20) Ishikawa, A.; Tanaka, T. J. Two-Photon Fabrication of Three-Dimensional Metallic Nanostructures for Plasmonic Metamaterials. *Laser Micro Nanoeng.* **2012**, *7*, 11–15.
- (21) Chen, C. C.; Hsiao, C. T.; Sun, S.; Yang, K. Y.; Wu, P. C.; Chen, W. T.; Tang, Y. H.; Chau, Y. F.; Plum, E.; Guo, G. Y. Fabrication of Three Dimensional Split Ring Resonators by Stress-Driven Assembly Method. *Opt. Express* **2012**, *20*, 9415–9420.
- (22) Dickson, R. M.; Lyon, L. A. Unidirectional Plasmon Propagation in Metallic Nanowires. *J. Phys. Chem. B* **2000**, *104*, 6095–6098.
- (23) Lee, T. H.; Dickson, R. M. Single-Molecule LEDs from Nanoscale Electroluminescent Junctions. *J. Phys. Chem. B* **2003**, *107*, 7387–7390.
- (24) Chen, I.-W. P.; Fu, M.-D.; Tseng, W.-H.; Yu, J.-Y.; Wu, S.-H.; Ku, C.-J.; Chen, C.-H.; Peng, S.-M. Conductance and Stochastic Switching of Ligand-Supported Linear Chains of Metal Atoms. *Angew. Chem. Int. Edit.* **2006**, *45*, 5814–5818.
- (25) Chae, D.-H.; Berry, J. F.; Jung, S.; Cotton, F. A.; Murillo, C. A.; Yao, Z. Vibrational Excitations in Single Trimetal-Molecule Transistors. *Nano Lett.* **2006**, *6*, 165–168.
- (26) Tsai, T.-W.; Huang, Q.-R.; Peng, S.-M.; Jin, B.-Y. Smallest Electrical Wire Based on Extended Metal-Atom Chains. *J. Phys. Chem. C* **2010**, *114*, 3641–3644.
- (27) Peng, S.-M.; Wang, C.-C.; Jang, Y.-L.; Chen, Y.-H.; Li, F.-Y.; Mou, C.-Y.; Leung, M.-K. J. One-Dimensional Metal String Complexes. *Magn. Magn. Mater.* **2000**, *209*, 80–83.
- (28) Pantazis, D. A.; McGrady, J. E. A Three-State Model for the Polymorphism in Linear Tricobalt Compounds. *J. Am. Chem. Soc.* **2006**, *128*, 4128–4135.
- (29) Wu, L.-P.; Field, P.; Morrissey, T.; Murphy, C.; Nagle, P.; Hathaway, B.; Simmons, C.; Thornton, P. Crystal Structural and Electronic Properties of Dibromo- and Dichloro-tetrakis[μ -3-bis(2-pyridyl)amido]tricopper (II) Hydrate. *J. Chem. Soc., Dalton Trans.* **1990**, 3835–3840.
- (30) Aduldecha, S.; Hathaway, B. Crystal Structure and Electronic Properties of Tetrakis[μ -3-bis(2-pyridyl)amido]dichlorotricopper(II)-water-acetone (1/0.23/0.5). *J. Chem. Soc., Dalton Trans.* **1991**, 993–998.
- (31) Pyrka, G. J.; El-Mekki, M.; Pinkerton, A. A. Structure of the Linear Trinuclear Copper Complex, Dichlorotetrakis-(di-2-pyridylamido)tricopper. *J. Chem. Soc., Chem. Commun.* **1991**, 84–85.
- (32) Shen, Y.; Jin, B. Y. Correspondence between Gentile Oscillators and N-Annulenes. *J. Phys. Chem. A* **2013**, *117*, 12540–12545.
- (33) Shen, Y.; Dai, W. S.; Xie, M. Intermediate-Statistics Quantum Bracket, Coherent State, Oscillator, and Representation of Angular Momentum [SU(2)] Algebra. *Phys. Rev. A* **2007**, *75*, 042111.
- (34) Shen, Y.; Ai, Q.; Long, G. L. The Relation between Properties of Gentile Statistics and Fractional Statistics of Anyon. *Physica A* **2010**, *389*, 1565–1570.
- (35) Greenwood, H. H. *Computing Methods in Quantum Organic Chemistry*; Wiley-Interscience: Weinheim, Germany, 1972.
- (36) Fleming, G. R.; Wolynes, P. G. Chemical Dynamics in Solution. *Phys. Today* **1990**, *43*, 36–43.
- (37) Salem, L. *The Molecular Orbital Theory of Conjugated Systems*; W. A. Benjamin: New York, 1966.
- (38) Bohm, D. *Quantum Theory*; Dover: New York, 1989.
- (39) Szabo, A.; Ostlund, N. S. *Modern Quantum Chemistry, Introduction to Advanced Electronic Structure Theory*; Dover: New York, 1996.
- (40) Bohm, A. *Quantum Mechanics: Foundations and Applications*; Springer, 3rd rev. and enlarged ed. 1993.
- (41) Smith, D. R.; Padilla, W. J.; Vier, D. C.; Nemat-Nasser, S. C.; Schultz, S. Composite Medium with Simultaneously Negative Permeability and Permittivity. *Phys. Rev. Lett.* **2000**, *84*, 4184–4187.

(42) Marqus, R.; Martel, J.; Mesa, F.; Medina, F. Left-Handed-Media Simulation and Transmission of EM Waves in Subwavelength Split-Ring-Resonator-Loaded Metallic Waveguides. *Phys. Rev. Lett.* **2002**, *89*, 183901.

(43) Decoopman, T.; Vanbesien, O.; Lippens, D. Demonstration of Backward Wave in a Single Split Ring Resonator and Wire Loaded Finline. *IEEE Microwave Wireless Compon. Lett.* **2004**, *14*, 507–509.

(44) García-García, J.; Bonache, J.; Gil, I.; Martín, F.; Marqus, R.; Falcone, F.; Lopetegi, T.; Laso, M. A. G.; Sorolla, M. Comparison of Electromagnetic Band Gap and Split-Ring Resonator Microstrip Lines as Stop Band Structures. *Microwave Opt. Technol. Lett.* **2005**, *44*, 376–379.

(45) Shamonin, M.; Shamonina, E.; Kalinin, V.; Solymar, L. Resonant Frequencies of a Split-Ring Resonator: Analytical Solutions and Numerical Simulations. *Microwave Opt. Technol. Lett.* **2005**, *44*, 133–136.

(46) Moser, H. O.; Casse, B. D. F.; Wilhelmi, O.; Saw, B. T. Terahertz Response of a Microfabricated Rod-Split-Ring-Resonator Electromagnetic Metamaterial. *Phys. Rev. Lett.* **2005**, *94*, 063901.

(47) Baena, J. D.; Bonache, J.; Martín, F.; Sillero, R. M.; Falcone, F.; Lopetegi, T.; Laso, M. A. G.; García-García, J.; Gil, I.; Portillo, M. F.; et al. Equivalent-Circuit Models for Split-Ring Resonators and Complementary Split-Ring Resonators Coupled to Planar Transmission Lines. *IEEE Trans. Microwave Theory Tech.* **2005**, *53*, 1451–1461.

(48) Aydin, K.; Bulu, I.; Guven, K.; Kafesaki, M.; Soukoulis, C. M.; Ozbay, E. Investigation of Magnetic Resonances for Different Split-Ring Resonator Parameters and Designs. *New J. Phys.* **2005**, *7*, 168–174.

(49) Zhou, J.; Koschny, Th.; Kafesaki, M.; Economou, E. N.; Pendry, J. B.; Soukoulis, C. M. Saturation of the Magnetic Response of Split-Ring Resonators at Optical Frequencies. *Phys. Rev. Lett.* **2005**, *95*, 223902.

(50) Rockstuhl, C.; Zentgraf, T.; Guo, H.; Liu, N.; Etrich, C.; Loa, I.; Syassen, K.; Kuhl, J.; Lederer, F.; Giessen, H. Resonances of Split-Ring Resonator Metamaterials in the Near Infrared. *Appl. Phys. B: Lasers Opt.* **2006**, *84*, 219–227.

(51) Guo, H.; Liu, N.; Fu, L. W.; Meyrath, T. P.; Zentgraf, T.; Schweizer, H.; Giessen, H. Resonance Hybridization in Double Split-Ring Resonator Metamaterials. *Opt. Express* **2007**, *15*, 12095–12101.

(52) Gwinner, M. C.; Koroknay, E.; Fu, L. W.; Patoka, P.; Kandulski, W.; Giersig, M.; Giessen, H. Periodic Large-Area Metallic Split-Ring Resonator Metamaterial Fabrication Based on Shadow Nanosphere Lithography. *Small* **2009**, *5*, 400–406.

(53) Aydin, K.; Cakmak, A. O.; Sahin, L.; Li, Z.; Bilotti, F.; Vegni, F.; Ozbay, E. Split-Ring-Resonator-Coupled Enhanced Transmission through a Single Subwavelength Aperture. *Phys. Rev. Lett.* **2009**, *102*, 013904.

(54) Decker, M.; Linden, S.; Wegener, M. Coupling Effects in Low-Symmetry Planar Split-Ring Resonator Arrays. *Opt. Lett.* **2009**, *34*, 1579–1581.

(55) Klessinger, M.; Michl, J. *Excited States and Photochemistry of Organic Molecules*; VCH Publishers, Inc.: Weinheim, Germany, 1995.

(56) Platt, J. Electronic Structure and Excitation of Polyenes and Porphyrins. In *Radiation Biology*; Hollaender, A., Brues, A. M., Eds.; McGraw-Hill: New York, 1956; Vol. 3, pp 71–123.

(57) Platt, J. Comparison of Classical and Quantum-Mechanical Light Absorption by Large Molecules or Small Particles. *Lowell Obs. Bull.* **1960**, *8*, 278–284.

(58) Mineo, H.; Yamaki, M.; Teranishi, Y.; Hayashi, M.; Lin, S. H.; Fujimura, Y. Quantum Switching of π -Electron Rotations in a Nonplanar Chiral Molecule by Using Linearly Polarized UV Laser Pulses. *J. Am. Chem. Soc.* **2012**, *134*, 14279–14282.

(59) Kanno, M.; Kono, H.; Fujimura, Y.; Lin, S. H. Nonadiabatic Response Model of Laser-Induced Ultrafast π -Electron Rotations in Chiral Aromatic Molecules. *Phys. Rev. Lett.* **2010**, *104*, 108302.